The effect of changes in the Earth's moment of inertia during glaciation on geomagnetic polarity excursions and reversals: Implications for Quaternary chronology

Rob Westaway

16 Neville Square, Durham DH1 3PY, UK

Geomagnetic polarity reversals and excursions in the Quaternary correlate well with interglacial-to-glacial transitions and glacial maxima. It is suggested that this relationship results from interactions between the Earth's mantle and core that accompany decreases in the Earth's moment of inertia during ice accumulation, which weaken the geomagnetic field in order to try to counter the decrease in differential rotation between the mantle and inner core that is being forced. In the Late Pleistocene, geomagnetic excursions directly correlate with brief phases of rapid ice growth that accompany falls in global sea-level, notably during the Younger Dryas stage, Dansgaard–Oeschger interstadials 5 and 10 that precede the rapid melting events during Heinrich events H3 and H4, and during the transitions between oxygen isotope stages 5c-5b, and 5e-5d. It is proposed that similar relationships between instabilities in climate and the geomagnetic field also typefied the Middle Pleistocene. As a result of the transfer of some of the mass of the oceans into polar ice sheets, the climate instabilities that initiate these rapid ice accumulations redistribute angular momentum and rotational kinetic energy between the Earth's mantle and inner core. These changes weaken the Earth's magnetic field, facilitating geomagnetic excursions and also causing enhanced production of cosmogenic nuclides, including ^{14}C. The subsequent phases of rapid ice melting, Heinrich events, reverse this effect: strengthening the field. This explanation, of forcing of geomagnetic excursions by climate instabilities, provides a natural explanation for why, during the Middle-Late Pleistocene, excursions have been numerous but none has developed into a polarity reversal: the characteristic duration of the climate instabilities is too short. River terrace aggradation, in Europe at least, is also likely to be concentrated during Heinrich events. The most important of these can now be dated throughout the Middle and Late Pleistocene, as they are expected to lag the geomagnetic excursions by no more than ~2 ka. Timings of these fluvial aggradations could also be constrained by observation of *in situ* production spikes of cosmogenic nuclides such as ^{10}Be, which would allow direct correlation with the geomagnetic excursions.

MANY reversals of the geomagnetic field are evident in the geological record. This field is generated in the Earth's liquid outer core, which is an electrical conductor that is convecting in order to transport heat upward. Numerical simulations[1] indicate that the observed[2,3] differential rotation between the solid inner core and mantle, by one part in $\sim 10^5$, is necessary for generation of a stable geomagnetic field. Because the convection in the outer core is vigorous, and thus, chaotic, one view has been that this tendency for field reversal is the spontaneous behaviour of a chaotic system[4–6]. In contrast, other studies[7–12] have suggested that the reduction in moment of inertia of the Earth that accompanies ice sheet growth, and is also one part in $\sim 10^5$, may increase the rotation rate of the mantle and thus trigger geomagnetic reversals or excursions.

This study re-examines the idea that geomagnetic polarity reversals and excursions can be caused by increases in the rotation rate of the mantle due to increases in the volume of polar ice sheets, which redistribute part of the mass of the oceans nearer the Earth's rotation axis and thus decrease its total moment of inertia. The underlying physics is similar to the familiar observation that, if a skater is spinning and pulls her arms in, towards her spin axis, her rate of rotation will increase. Increasing the rotation rate of the mantle in this manner will bring it closer to the pre-existing rotation rate of the inner core, which is shown to weaken and thus de-stabilize the geomagnetic field. This idea is reassessed in the light of modern magnetostratigraphic and oxygen-isotope data sets[13–16], orbitally-tuned chronologies[17,18], and recent advances in knowledge of the magnetohydrodynamics of the Earth's core[1–3]. The immediate aim is to establish the chronological correlations which lead to the proposed series of cause-and-effect relationships, for use as a high-resolution dating tool.

e-mail: r.w.c.westaway@ncl.ac.uk

My interest in these issues developed through involvement in physical modelling of Quaternary uplift revealed by the incision of long-term river terrace sequences[19–22]. Along major rivers in Europe, one often observes one terrace for each of the most recent climate cycles, with sequences sometimes dating back to the Late Pliocene or earlier[23,24]. However, the phase relationship between glacial cycles and terrace formation has proved difficult to resolve: for instance, it has required much effort to establish whether aggradation and incision are concentrated around glacial maxima and interglacials, or, as now favoured, during transitions to and from periglacial conditions[19,25,26]. Where terrace sequences are magnetostratigraphically dated, one typically observes most of the known polarity reversals between the Gauss chron and the present day, either in silts intercalated within terrace gravels or in palaeosols which cap terraces[24]. This seems remarkable, given that river terrace records are fragmentary, and suggests the possibility of a characteristic phase relationship between geomagnetic instabilities and times of terrace formation.

One also observes sequences of terraces[21–27] which are very similar to each other (in gradient, thickness, composition, etc.), although conditions varied dramatically during different climate cycles (for instance, biostratigraphic evidence indicates that some interglacials were much warmer than others; some glacials involved growth of major ice sheets in Europe, others did not). In addition, one often observes terraces that can only have formed during minor cold stadials (or transitions into them), and yet they appear no different from others in the same sequence that are dated to whole climate cycles. Examples are in oxygen isotope stage (OIS) 7b (~ 190 ka), 13b (~ 480 ka), and 15b (~ 600 ka)[20–22,27] (Figure 1). River terraces aggrade at times of high sediment input into river systems. Recent syntheses of evidence[19,25] establish that, in north-west Europe, this can occur during either warming or cooling limbs when enough seasonal rainfall or melt-water is present to mobilize sediment, which is made easily transportable by the relative lack of vegetation. However, these syntheses offer no insight into precisely when in each climate cycle these conditions are expected, information that also cannot normally be obtained directly from the terraces themselves as they usually lack material capable of being dated using any conventional technique.

Global ice volume does not fluctuate at steady rates[28–32]. The oxygen isotope variations in Figure 1 instead form a running average of shorter-term fluctuations, some as short as ~ 1 ka: the Dansgaard–Oeschger cycles. These involve alternations of strong and weak thermohaline circulation in the North Atlantic ocean. When strong, this circulation transports warm water to north polar regions. Evaporation facilitates snowfall and ice accumulation on adjacent land. The resulting ice advances lead to calving of icebergs and rapid melting. These alternations of rapid melting – Heinrich events – release enough low-density melt-water to disrupt the thermohaline circulation in the North Atlantic. The Gulf Stream thus shuts down, and the resulting high-latitude cooling terminates the melting event, allowing the thermohaline circulation to later re-establish. In the meantime, the shutdown of the Gulf Stream causes the polar climate front to move southward to the vicinity of Europe. This will cause local cooling (which will reduce vegetation), with high precipitation along the polar front[33,34] – precisely the conditions identified earlier as conducive to river terrace formation.

In its simplest form, the proposed coupling relationship between ice volume and geomagnetic instabilities predicts that the geomagnetic field is expected to be weakest, facilitating excursions or reversals, at times of greatest ice volume. This may have been the main effect during the Early Pleistocene (Figure 2). However, this is evidently not so for the Middle and Late Pleistocene, when there has been no correlation between the strength of the geomagnetic field (VADM) and ice volume (Figure 2). This study thus suggests a more complex hypothesis linking these and related processes, in which for the Middle and Late Pleistocene the most important effect on the geomagnetic field has not been from the total ice volume: it results instead from the high rates of change of ice volume caused by Dansgaard–Oeschger climate instabilities.

Numerical simulations of the Earth's core[1,35–38] allow internally consistent solutions of the equations governing the flow regime and poloidal and toroidal components of the magnetic field (Figure 3). These simulations indicate, for instance, that the flow is predominantly eastward near the inner core boundary (ICB). This exerts viscous and magnetic torques on the inner core, which create a characteristic situation in which the inner core is in equilibrium when rotating faster than the mantle. Furthermore, because the inner and outer core are electrical conductors, the magnetic field within them cannot change arbitrarily. In particular, this field can only diffuse into or out from the solid inner core relatively slowly. The characteristic time scale for the field to change significantly within the inner core is estimated[5] as ~ 3 ka. To crudely summarize a very complex situation, numerical simulation indicates that the flow in the outer core is constantly trying to reverse the polarity of the field on the short (~ 100 year) characteristic time scale of its convective circulation. Most such attempts fail because the field in the solid inner core usually has insufficient time to diffuse away before more field of the same polarity is regenerated at the ICB. However, occasionally, the combination of flow and magnetic fields in the outer core retains the correct form to induce a polarity reversal for long enough for the original axial dipole field in the inner core to diffuse away completely. When this happens, a dipole field of the opposite polarity can then diffuse into the inner core, thus stabilizing this opposite polarity in the future. Once

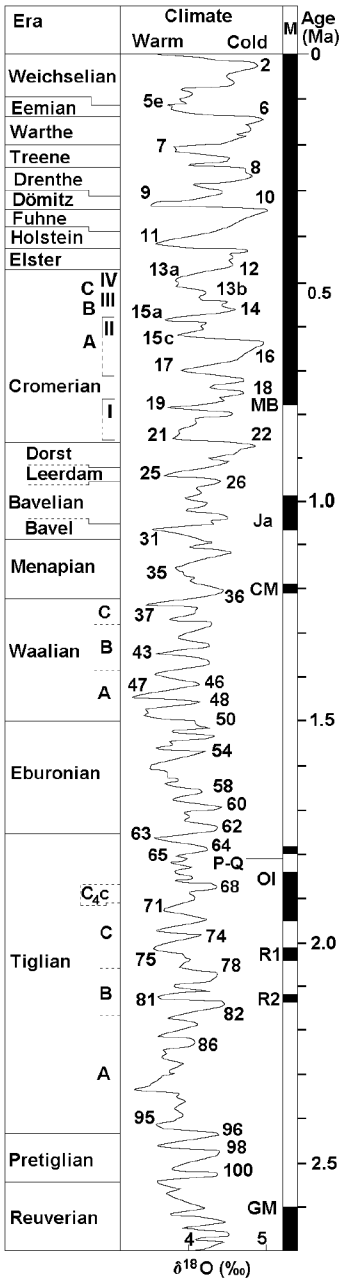

Figure 1. Graph of benthic $\delta^{18}O$ against time since the Late Pliocene, for ODP site 677, originally from ref. 17, showing magnetic polarity reversals and stratigraphic stages for north-western Europe. Adapted from figure 5 of ref. 22 and figure 7 of ref. 20.

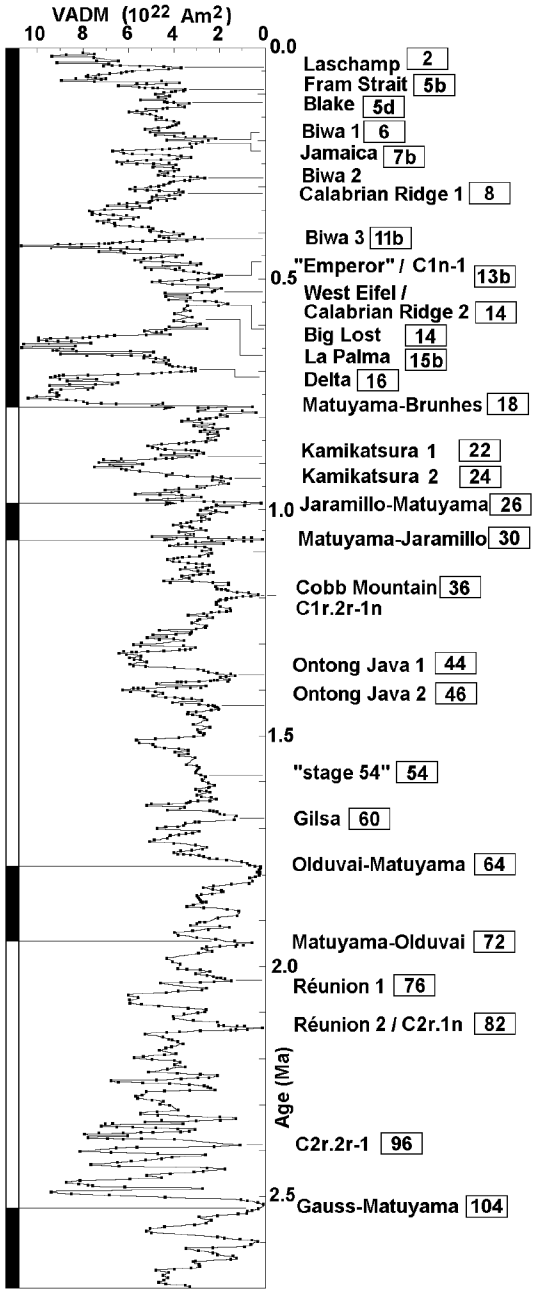

Figure 2. Graph of the Earth's estimated Virtual Axial Dipole Moment (VADM) against time, based on palaeointensity measurements from ODP sites 848 and 851. Adapted from figure 3 of ref. 13, with ages of geomagnetic events added from the literature[13–18,41,42,44,46,68–73].

the dipole field component with this opposite polarity is established in the inner core, the twisting effect of the flow in the inner part of the outer core strengthens it at the expense of the toroidal field, and the polarity reversal is complete. It is thus evident[5] that a geomagnetic reversal requires these conditions to be maintained in the outer core for a typical time-scale of at least ~3 ka, to allow time for the field with the new polarity to diffuse into the inner core. If these conditions are maintained for less time, only an excursion will result, and the field will subsequently return to its original polarity.

Figure 4 shows the variations with time of the kinetic energy of the convection in the outer core and the total energy stored in the magnetic field, for the simulation in Figure 3. Both quantities are fluctuating constantly. At one point, these fluctuations in combination produce a

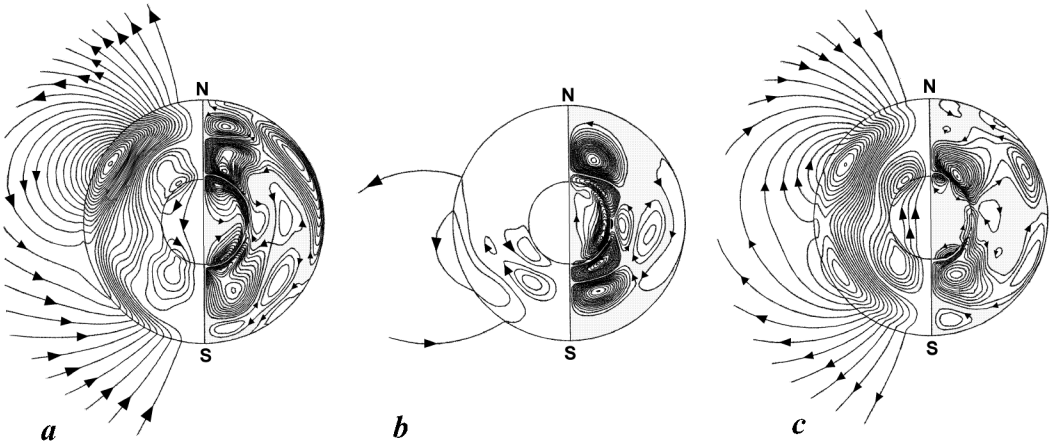

Figure 3. The structure of the geomagnetic field during a reversal from R to N polarity, from a numerical simulation[35]. Figure parts show (***a***) before, (***b***) during, and (***c***) after the reversal. At each stage, the left half of the figure shows the poloidal component of the field (i.e. the component in the vertical plane) and the right half shows the toroidal (i.e. azimuthal, or longitudinal) component, both components being averaged azimuthally (i.e. over longitude). The ICB and CMB are indicated, and lines of force of the poloidal field are shown to the Earth's surface with directions indicated conventionally. At each point, greater strength of the poloidal field is indicated by closer spacing of the lines of force. Contour lines indicate strength of the toroidal component, which is confined to the core, with arrowhead symbols indicating its direction, in accordance with a right-hand rule (thus, if arrowheads point clockwise along contour lines, the toroidal field is directed out of the plane of the page, and is thus oriented eastward). Grey shading marks localities where the toroidal field is near zero. Before the reversal (***a***), the poloidal component of the magnetic field consists of a dipole with *R* polarity outside the outer core and in the outer part of the outer core, plus another dipole with the opposite polarity in the inner core and inner part of the outer core. (***b***), This shows the moment of reversal as seen at the ICB. The reversal as measured from the VADM minimum at the Earth's surface will lag behind this by ~1 ka (ref. 35). At the moment depicted, the poloidal field is weak everywhere, but still retains its original polarity at the Earth's surface near the equator. Thus an unsuccessful attempt at reversal (i.e. an excursion) may result in a temporary polarity reversal near the poles but maintaining a uniform polarity near the equator. However, the toroidal field component is stronger than before and has the same direction (westward) throughout the inner core and the inner part of the outer core, unlike before and after the reversal when it had opposite directions in the two hemispheres. (***c***) After the reversal the field is similar to before the reversal, at this stage comprising a dipole with *N* polarity in the mantle and outer part of the outer core. Adapted from figure 1 of ref. 35. The figure parts depicted here represent snapshots of the fluctuations summarized in figure 4 at times of 31 ka (***a***), 36 ka (***b***) and 40 ka (***c***) into the model.

peak in the kinetic energy associated with the convective motion in the outer core, and a reduction in the magnetic energy. The resulting weakening of the magnetic field allows a reversal to occur. In the original simulation[35,36], this combination of all values being 'right' for a reversal arose by chance. Below, it is suggested that ice sheet growth can also cause weakening of the geomagnetic field, likewise facilitating a 'forced' excursion or reversal.

The rotational response to ice sheet growth

The moment of inertia of the crust and mantle, I_m, is roughly $(8\pi/15)\rho_m\ (R_c^5 - R_o^5)$ with ρ_m the density of the mantle, and R_e and R_o the radii of the Earth and outer core. With ρ_m 4000 kg m^{-3}, R_e 6370 km, and R_o 3490 km, one obtains I_m 6.7×10^{37} kg m^2. The moment of inertia of the water mass that forms part of the oceans during each interglacial but is bound up in ice sheets during glacials, is designated as I_w. It can be estimated from the ~120-m global sea level fall during the last glacial maximum[39]. Since the sea occupies ~2/3 of the Earth's surface, this water mass can be approximated as a spherical shell of radius R_e and thickness, h, 80 m. Taking its density, ρ_w, as 1000 kg m^{-3}, the mass M_w of this water layer can be estimated as $4\pi\rho_w R_e^2 h$, and is $\sim 4 \times 10^{19}$ kg. Using the formula for a spherical shell, (2/3) M_w R_e^2, its moment of inertia I_w, is thus $\sim 1.1 \times 10^{33}$ kg m^2. When this water mass is bound up in northern hemisphere ice sheets, its moment of inertia I_s can be estimated using the formula for a disk, (1/2) M_w R^2. Taking the effective radius R of this disk as ~2000 km, I_s is $\sim 8 \times 10^{31}$ kg m^2.

Thus, during the transition to a glacial, the moment of inertia of the outer part of the Earth changes from $I_m + I_w$ to $I_m + I_s$, a decrease by ~1/67000 or $\sim 1.5 \times 10^{-5}$ of its initial value. Neglecting for the time being any torque acting on the mantle due to viscous or magnetic coupling with the core, the angular momentum of the outer part of the Earth (its moment of inertia I multiplied by its angular velocity ω) will be conserved. As a result, its rotation rate ω would increase by $\sim 1.5 \times 10^{-5}$ of its initial value. The moment of inertia of the inner core I_i can be estimated[1] as 5.86×10^{34} kg m^2, using the standard equation for a sphere: $I_i = (2/5)\ M_i\ R_i^2 = (8\pi/15)\ \rho_i\ R_i^5$ with R_i 1220 km and ρ_i ~13000 kg m^{-3}. Given that its angular velocity, ω, is ~0.663 mrad s^{-1} (i.e., ~360° per day), its rotational kinetic energy (1/2 $I\omega^2$), is 1.29×10^{28} J.

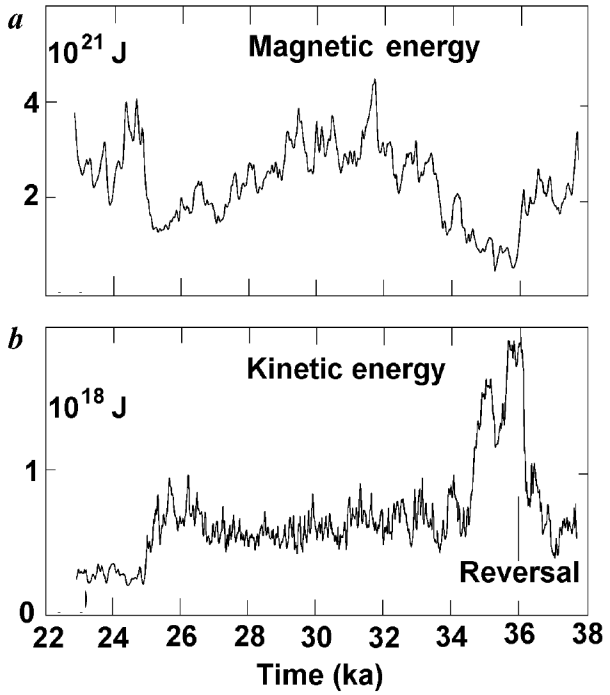

Figure 4. Fluctuations in (***a***) magnetic energy and (***b***) kinetic energy for the outer core predicted by a numerical simulation. The figure shows conditions between 20 and 40 ka after the start of the simulation, which by this time has ceased to depend on the assumed initial conditions. A simulated polarity reversal occurs at 36 ka, marked by a maximum in kinetic energy that is due mainly to a relatively high rate of differential rotation and a weakening of the field indicated by the reduction in magnetic energy. Adapted from figure 1 of ref. 36.

Suppose that, when a mass M of water is abruptly transported from an initial position forming a spherical shell at the Earth's surface to a final position in a polar ice sheet, the angular velocities of the mantle and inner core change from ω_{om} to ω_{1m} and ω_{oi} to ω_{1i}. No external torque acts, so total angular momentum is conserved, and

$$(I_m + I_w)\omega_{mo} + I_i\omega_{io} = (I_m + I_s)\omega_{m1} + I_i\,\omega_{i1}. \quad (1)$$

Work W needs to be done to move the mass M of water closer to the rotation axis. The required energy input comes from the climate system. After some algebra one may estimate:

$$W = \frac{M\omega_{mo}^2}{12}(4R_e^2 - 3cR_d^2), \quad (2)$$

where R_e is the radius of the Earth, R_d is the radius of the disk used to represent the polar ice sheet, and c is a factor determined by the profile of this ice sheet. If total energy (rotational kinetic energy plus energy stored in the Earth's magnetic field) is otherwise conserved, then

$$(I_m + I_w)\omega_{mo}^2 + I_i\omega_{io}^2 + 2\Delta E_\mu + 2W = (I_m + I_s)\omega_{ml}^2 + I_i\omega_{il}^2, \quad (3)$$

Table 1. Energy and angular momentum calculations

Quantity	Units	Solution 1	Solution 2
Input parameters			
M	kg	1×10^{18}	-6×10^{17}
ΔI_w	kg m^2	-2.75×10^{31}	1.65×10^{31}
ΔI_s	kg m^2	2.60×10^{30}	-1.56×10^{30}
ω_{mo}	μrad s^{-1}	72.722052	72.722052
ω_{io}	μrad s^{-1}	72.723711	72.723711
$\Delta\Omega_o$	μrad s^{-1}	0.001659	0.001659
ΔE_μ	J	-6.24721×10^{20}	3.74856×10^{20}
Derived parameters			
ω_{m1}	μrad s^{-1}	72.722079	72.722036
ω_{i1}	μrad s^{-1}	72.723738	72.723695
$\Delta\Omega_1$	μrad s^{-1}	0.001659	0.001659
$\Delta\omega_m$	μrad s^{-1}	0.000027	−0.000016
$\Delta\omega_i$	μrad s^{-1}	0.000027	−0.000016
ΔE_m	J	6.57267×10^{22}	-3.94360×10^{22}
ΔE_i	J	1.15081×10^{20}	-6.90592×10^{19}
ΔL_m	N m s	-1.58244×10^{24}	9.49611×10^{23}
ΔL_i	N m s	1.58244×10^{24}	-9.49611×10^{23}

Most symbols are defined in the text, with M as the mass of water transferred from ocean to ice sheet, $\Delta\omega_m = \omega_{m1} - \omega_{mo}$, and $\Delta\omega_i = \omega_{i1} - \omega_{io}$. ΔE_m, ΔL_m, ΔE_i, and ΔL_i are the changes in rotational kinetic energy and angular momentum for the mantle and inner core, respectively. $\Delta\Omega o$ ($= \omega_{io} - \omega_{mo}$) and $\Delta\Omega_1$ ($= \omega_{i1} - \omega_{m1}$) are the differential rotation between the inner core and mantle before and after the imposed change. Calculations use equations and parameter values listed in the text. See text for discussion.

where ΔE_μ is the change in energy stored in the magnetic field.

Combining eqs (1) and (3) gives

$$\omega_{ml} = \frac{(I_m + I_s)(I_i\omega_{io} + (I_m + I_w)\omega_{mo}) - \sqrt{D}}{(I_m + I_s)(I_i + I_m + I_s)}, \quad (4)$$

where

$$\begin{aligned} D = {} & 2(W + \Delta\dot{A}_\mu)(\dot{E}_m + \dot{E}_s)(I_i + I_m + I_s)I_i \\ & + (I_m + I_s)I_i^2 I_m(\omega_{io} - \omega_{mo})^2 + \omega_{io}^2 I_i^2 I_s(I_m + I_s) \\ & + [(I_m + I_s)(I_m I_s + I_i I_w) - (I_w - I_s)I_s I_w \\ & - (I_m + I_w)I_m I_w]I_i\omega_{mo}^2 \\ & - 2(I_m + I_s)I_i^2 I_w\omega_{io}\omega_{mo}. \end{aligned} \quad (5)$$

These equations allow one to specify changes to I_s and I_w, then look for the required change ΔE_μ assuming the mantle and inner core maintain constant differential rotation. In solution 1 (Table 1) a water mass M of 10^{18} kg is abruptly transferred from ocean to polar ice sheet, consistent with an abrupt fall in global sea-level of ~3 m, as may be expected during the phase of a Dansgaard–Oeschger cycle with strong thermohaline circulation (see below). To maintain constant differential rotation requires the energy E_μ stored in the geomagnetic field to decrease by $\sim 6 \times 10^{20}$ J. Given[36] that E_μ is typically $\sim 10^{21}$ J in a stable situation (Figure 4), such a change

would cause a substantial weakening in the field. The physical reason for this decrease in magnetic energy is that energy initially present in the magnetic field does work against both the mantle and inner core to try to maintain a stable differential rotation while the water mass is redistributed. The solutions indeed indicate that if ΔE_μ is assumed to be zero, this redistribution will cause a slight decrease in the rotation rate of the mantle and a dramatic increase in the rotation rate of the inner core. However, when ΔE_μ is $\sim -6 \times 10^{20}$ J, the same mass redistribution causes small increases in both these rotation rates.

If the same water mass is restored to the ocean, the calculations indicate that a corresponding increase in E_μ will restore the original rotation rates of both the mantle and inner core, as is expected. However, if only 60% -6×10^{17} kg of water – is restored, equivalent to a ~ 2 m rise in sea-level, calculations (solution 2 in Table 1) indicate that the same differential rotation is maintained with $\sim 4 \times 10^{20}$ J of energy restored to the magnetic field. The overall effect of this sea-level fall and subsequent rise would thus be a net reduction in the energy stored in the Earth's magnetic field by 2×10^{20} J, and an increase in the rotation rate of the mantle by ~ 15 parts in 10^8– equivalent to a reduction in the length of the day by ~ 0.01 s.

Patterns in palaeomagnetic data and their implications

Comparison of the age-control evidence in Figures 1 and 2 indicates that all 15 geomagnetic excursions during the Brunhes chron have occurred at times of ice-sheet growth. Other excursions back to the Matuyama–Jaramillo reversal also follow the same pattern. However, most earlier excursions and reversals occur during (or shortly before) glacial maxima.

During the early and middle Matuyama chron, the concentration of geomagnetic excursions at glacial maxima suggests that the main underlying physical mechanism was the overall reduction in magnetic energy as the mantle and inner core are both spun up during the transitions to glaciations. The resulting weakening of the field within the outer core means that each attempted reversal has a greater probability of succeeding at such a time, as already noted.

The oxygen isotope evidence (Figure 1) indicates that the typical amplitude of ice volume fluctuations at this time was about one third to one half that for the largest Middle and Late Pleistocene glaciations. Falls in global sea-level of ~ 40–60 m, and associated changes in moment of inertia of the order of ~ 4–6×10^{32} kg m^2, are thus indicated. Given the characteristic ~ 40 ka period of climate cycles, the typical duration of each phase of ice sheet growth was ~ 20 ka, indicating time-averaged rates of change of moment of inertia of the order of ~ 2–3×10^{28} kg m^2 yr^{-1} and rates of sea-level fall of ~ 2–3 mm a^{-1}. It is clear that, for much of the Late Pliocene and Early Pleistocene, the records of VADM (Figure 2) and δ^{18}O (Figure 1) are in phase and well-correlated, with VADM an effective proxy for δ^{18}O.

Oxygen isotope data[17] and other evidence[40] indicate that OIS 36 involved the first Quaternary glaciation with a global ice volume and associated sea-level fall (Figure 5) approaching the largest Middle–Late Pleistocene glaciations. The transition from geomagnetic events being typically at glacial maxima to being during phases of ice acumulation occurs at this time. This change in character is illustrated by the timing of the Matuyama–Jaramillo and Jaramillo–Matuyama reversals, both of which occurred shortly after interglacials (Figure 2). From this time on, no correlation has existed between VADM minima and glacial maxima: the VADM record is indeed dominated by much shorter-period fluctuations than the ~ 100 ka (eccentricity-driven) period of the climate. Although some interglacials (e.g. OIS 17, 15, 9, and 1) have involved high VADM, others (e.g. OIS 25 and 5e) have not.

However, it is evident that the Late Pleistocene oxygen isotope variations shown in Figure 1 form a running average of much shorter-term climate instabilities associated with the Dansgaard–Oeschger cycles (Figure 6), which include alternations of rapid melting – Heinrich events – and ice accumulation. It follows that on timescales of centuries to millennia in the Middle–Late Pleistocene, rates of ice accumulation and of decrease in moment of inertia may have been much greater than the overall time-averages during interglacial-to-glacial transitions. It is indeed notable that the Laschamp, Mono Lake, and Gothenburg excursions, the three youngest, all occurred just before Heinrich events (Figure 6).

The Laschamp excursion is dated[13,14,41–44] to a ~ 1 ka interval within ~ 40–44 ka, most likely[42,43] ~ 41 ka. It is marked[41,44,45] by abrupt increases in production rates of cosmogenic ^{10}Be, ^{36}Cl, and ^{14}C. It coincided[42] with Dansgaard–Oeschger interstadial (IS) 10 and preceded[28,32] the rapid melting during Heinrich event H4 and the subsequent IS 8 (Figure 6). The Mono Lake excursion (at 32 or 34 ka)[41,43], also associated with a ^{10}Be spike and increased ^{14}C production[41,44], matches IS 5 that preceded[28,32] the rapid melting during Heinrich event H3, before IS 4 (Figure 6). The Fram Strait and Blake excursions also occurred at times of ice growth, during the transitions to OIS 5b and 5d (Figure 6).

The Gothenburg excursion occurred in the early part of the Younger Dryas stage[46], the brief cooling within the transition from the last glacial maximum to the Holocene. Some studies[46,47] reported that the global sea level fell at this time by ~ 10 m for a few centuries before rising again as melting resumed: consistent with the observed growth of the Laurentian, Scandinavian, and Scottish ice sheets[48–52]. The widely-used Fairbanks[39] sea-level curve,

which shows no such fall, can indeed be modified to permit one, by ~5 m or more (Figure 5). If this involved a rate of sea-level fall of 25 mm a^{-1}, time-averaged over 200 years, the rate of change of moment of inertia was ~ 2.5×10^{29} kg m^2 yr^{-1}.

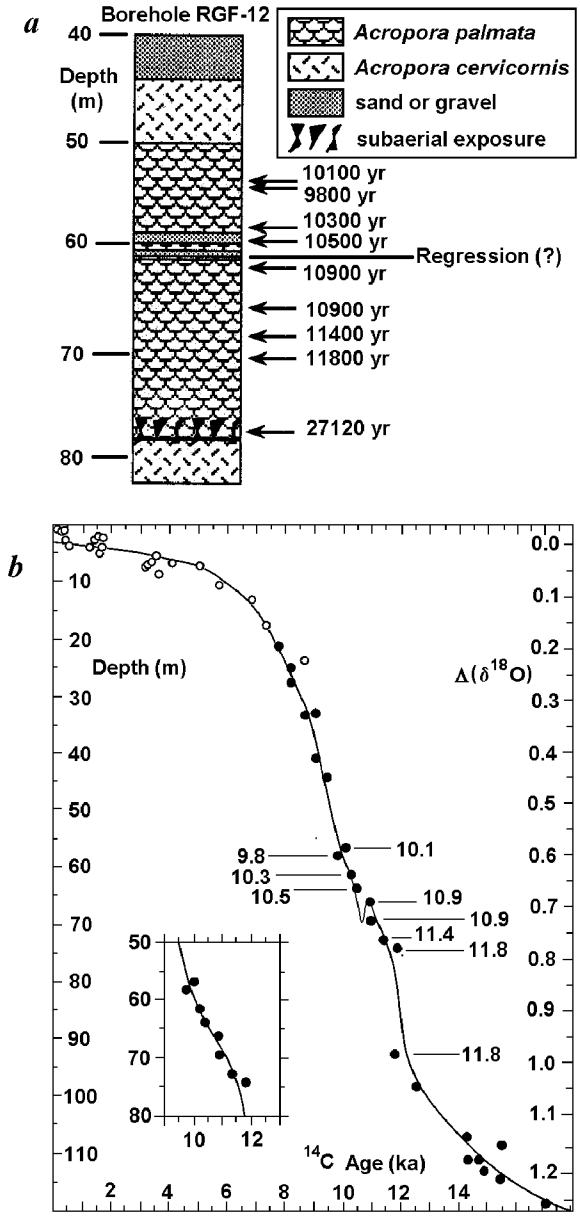

Figure 5. ***a***, The key data, from a borehole through coral offshore of Barbados, showing the hiatus in coral growth after 10.9 ka (uncalibrated radiocarbon years – uncorrected for secular variations in ^{14}C production; ~13 ka in calibrated years) that may mark a brief marine regression during the Younger Dryas event. Adapted from part of figure 1 of ref. 39. The key coral species *Acropora palmata* is a sensitive indicator of sea-level as it only grows within ~5 m of the sea surface. ***b***, Depth below present-day sea-level of the instantaneous sea surface as a function of age (in uncalibrated radiocarbon years) for coral offshore of Barbados (with samples from off other Caribbean islands indicated by open symbols), including the data in (***a***). The evidence permits a small (~5 m) fall in global sea-level during the Younger Dryas event. Inset shows the alternative interpretation, with monotonically increasing sea-level, from ref. 39. Adapted from figure 2 of ref. 39.

The Heinrich events involve climate deterioration in Europe, creating the conditions (reduced vegetation and increased rainfall) for river terrace aggradation. One can thus predict that the preceding geomagnetic instability should be preserved in temperate deposits from immediately beforehand. One thus has the basis of method for high-resolution dating of river terrace deposits in this region. Furthermore, the presence of frequent geomagnetic excursions in the late Early Pleistocene and Middle

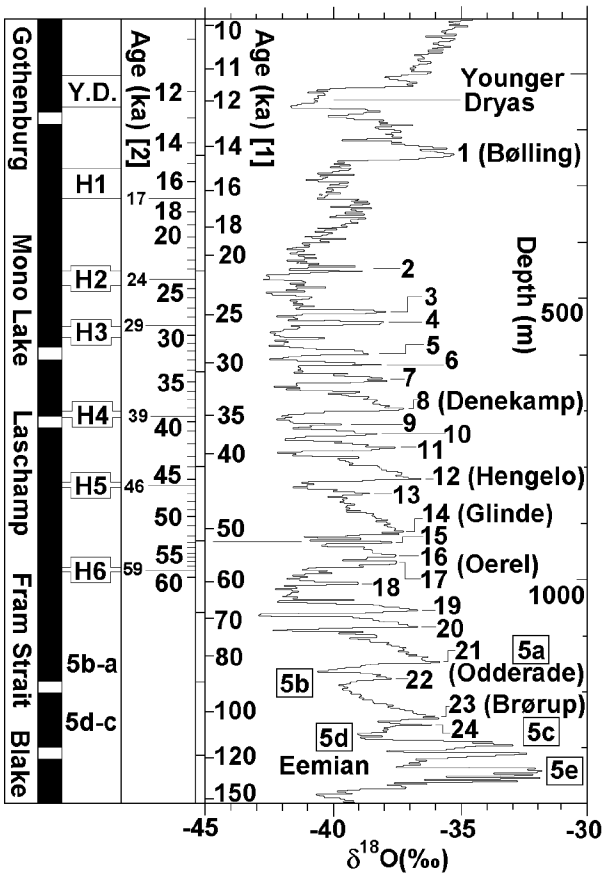

Figure 6. Chronology of the last glacial cycle. Comparison of the GRIP Greenland ice-core oxygen isotope record[28] and the series of numbered interstadials derived from it with the sequence of Heinrich events (H6 to H1, involving rapid melting of northern hemisphere ice sheets, plus Y.D., the rapid melting during and after Younger Dryas stage)[32] and the record of geomagnetic polarity excursions. Ages [1] and correlations with European interstadial names were assigned by ref. 28, [2] being obtained from ref. 32 by matching their ages obtained for the GISP2 ice core with corresponding oxygen isotope variations from the GRIP core. I note in passing that until quite recently, correlations between ice core and oceanic $\delta^{18}O$ records were considered problematic. Recognition of the Heinrich events and markers provided by volcanic ash layers now facilitate this correlation[31,42]. However, correlations with European interstadials remain tentative[66]: for instance, others[65,66] have dated the Hengelo and Denekamp interstadials to ~39–36 ka and ~32–28 ka, suggesting correlations as late as IS 8 and 4–3, not IS 12 and 8 as shown here. This would fit the patterns IS10 (Laschamp) → H4 → IS8 (Hengelo) and IS5 (Mono Lake) → H3 → IS4 (Denekamp). Note also that although Heinrich event H5 (at[42] 45.5 ka) did not follow a geomagnetic excursion, it did follow the interval ~48–46 ka, when the VADM decreased by ~50–70% of its previous value[43].

Pleistocene suggests that similar climate instabilities also occurred then, as well as in the Late Pleistocene. The proposed causal link between these excursions and Heinrich events suggests that similar climatic conditions developed each time, potentially explaining the observed similarity throughout the river terraces in each sequence in western Europe. Furthermore, OIS 15b, 13b and 7b each contained a geomagnetic excursion (the La Palma, 'Emperor', and Jamaica/Pringle Falls excursions: Figure 2), which can explain why these brief intervals have yielded river terraces comparable to those from major cooling limbs. The shortness of the Dansgaard–Oeschger climate instabilities, relative to the ~3 ka time scale[5] for field reversal, may also explain why they readily produce geomagnetic excursions but none has caused a reversal.

Cosmogenic nuclides such as ^{10}Be, ^{14}C, and ^{36}Cl are produced by cosmic-ray bombardment of the upper atmosphere. Weakening of the geomagnetic field (caused by these climate instabilities), which normally partially shields the upper atmosphere against such bombardment, provides a natural explanation[44,53] for the increased production rates of cosmogenic nuclides during geomagnetic excursions. There is thus no need to invoke other effects, such as supernovae, to explain these increases[41,54]. It has indeed been suggested[43,55] that production rates of ^{10}Be and ^{36}Cl are good proxies for VADM: observation of these nuclides in land surfaces immediately pre-dating river terraces may thus provide additional age control. One may also envisage 'calibrating' ^{14}C data[56] directly in terms of global ice volume and VADM.

It is also evident from Table 1 that an abrupt sea-level fall by ~120 m would extract more energy from the geomagnetic field than could ever be present to start with. This implies that another mechanism, not so far considered, operates to regenerate the field between smaller abrupt sea-level falls. The previous analysis assumed that rotation rates of the mantle can change arbitrarily, because it is an electrical insulator. However, it has been suggested[37] that it may instead behave as a weak conductor, possibly because its base is bonded to a thin layer of solid iron that has frozen out of the core. If so, the resulting weak electromagnetic coupling between the mantle and the Earth's magnetic field could gradually act to convert rotational kinetic energy of the mantle into magnetic energy, gradually regenerating the geomagnetic field between times of rapid sea-level fluctuations.

Other studies[57–59] have noted correlations between extinctions and geomagnetic reversals at many points in the geological record. The first suggested mechanism, that geomagnetic reversals cause extinctions because of increased cosmic ray irradiation of the Earth's surface when the field is weak[57], was shown to be untenable[60]. However, later work[58] established that many marine microfossil species have become extinct at geomagnetic reversals, notably during the Matuyama chron. An explanation is that both geomagnetic reversals and extinctions can be caused by rapid ice growth at times of rapid climate change. The extinctions may thus result because the climate changes so quickly that species cannot adapt, although it has been suggested[59] instead that the most important effect is a direct biochemical interaction of the geomagnetic field. For instance, the well-documented extinction in Europe of the ancient water vole *Mimomys savini* and its replacement by the species *Arvicola terrestris cantiana* is an important Middle Pleistocene marker[61], which probably[22] indicates OIS 14 that was not a major glaciation. This extinction may have instead marked a rapid climate deterioration, possibly the Heinrich event presumed to follow the Big Lost geomagnetic excursion during the transition to OIS 14 (Figure 2). Another example may be the extinction of many large mammal species around the time of the Younger Dryas event[59,62]. Others[46,63] have suggested that human subspecies introductions and cultural changes also correspond with geomagnetic instabilities. For instance, Neanderthals disappeared from much of Europe during the Würm II stadial that preceded the arrival of modern humans in the Hengelo interstadial[64]. Figure 6 suggests that this extinction occurred during Heinrich event H5, which directly followed a dramatic reduction in VADM[43]. However, an alternative chronology[65] (see Figure 6 caption) would place it during Heinrich event H4, which directly followed the Laschamp excursion[42]. This extinction thus apparently resulted from the inability of Neanderthals to cope with the deteriorating climate at this time. However, as others[66] previously noted, this example also illustrates that existing dating evidence may be too poor to establish definitive correlations with individual Dansgaard–Oeschger cycles, indicating the need for improved age control to fully test the hypothesis suggested in this paper.

Examples from the fluvial record

As already noted, the idea that instabilities in the geomagnetic field may correlate with times of river terrace formation has developed as a result of magnetostratigraphic study of fluvial deposits, notably those of the River Maas in the Netherlands[24]. The Maas has yielded what is, in many respects, the best long-term river terrace sequence currently known anywhere in Europe, with 31 terraces that date back probably to the Late Miocene[20,21,24] (Figure 7 *a*). A total of ~180 m of surface uplift since the Early Pliocene is thus indicated in this area (Figure 7 *b*, *c*). The uplift rate has fluctuated, being greatest in the Late Pliocene and Middle–Late Pleistocene, with a relative lull for most of the Early Pleistocene (Figure 7 *d*).

The characteristic pattern for most of the Matuyama chron, of instability in the geomagnetic field correlating with maxima in global ice volume that are represented by even OIS numbers, is well illustrated by the Simpelveld 1

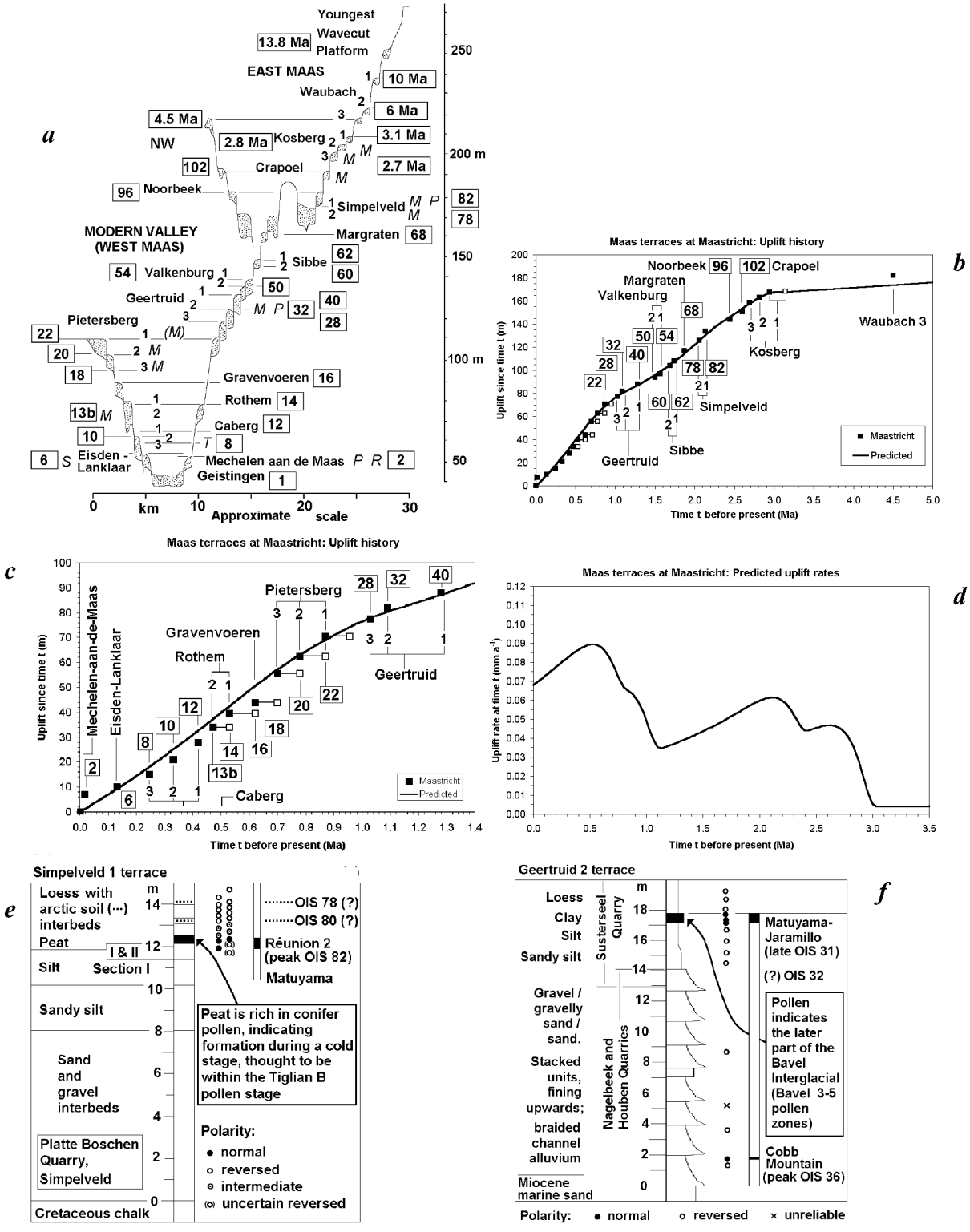

Figure 7. Evidence from the Maas terrace sequence in the Netherlands. (***a***) Transverse profile through the terrace staircase in the Maastricht area, adapted from figure 3 of ref. 20 (see also figure 3 of ref. 21 and figure 6 of ref. 24). Terrace alluvium is stippled. Italic letters indicate terraces with dating evidence: *M*, from magnetostratigraphy; *P*, from pollen; *R*, from radiocarbon dating; and *S*, from a soil profile. Age assignments to preferred oxygen isotope stages are indicated. (***b***) to (***d***) Observed and predicted uplift history ((***b***) and (***c***); (***c***) being an enlargement of (***b***), showing the Middle and Late Pleistocene in greater detail) and predicted variation in uplift rate (***d***). Predictions, based on figure 5 of ref. 21, use u 20°C km^{-1}, z_b 15.5 km, z_i 26 km, T_{e1} –10.0°C, T_{e2} –2.7°C, T_{e3} –1.7°C, T_{e4} –2.4°C, and T_{e5} –1.9°C (refs 20 and 22 define these parameters). Symbols in (***b***) and (***c***) indicate observed amounts of uplift estimated from altitudes of tops of river terraces relative to river level; open symbols indicate alternative ages that are not preferred. (***e***) and (***f***) Sedimentary and magnetostratigraphic evidence from (***e***) the Simpelveld 1 terrace and (***f***) the Geertruid 2 terrace. Adapted from parts of figures 8 and 9 of ref. 24. See ref. 24 for locations of the quarries that yielded these sections. See text for discussion.

terrace (Figure 7 *e*). This consists of a ~12 m thickness of fluvial deposits, which fine upwards, covered by a thin pollen-bearing peaty clay horizon, overlain by loess with arctic soil interbeds[24]. A brief interval of normal geomagnetic polarity, thought to represent the Réunion 2 subchron[24], is observed in the lower part of this peat horizon and in the uppermost part of the underlying fluvial silt (Figure 7 *e*). This evidence is entirely consistent with the interpretation that the fluvial sediments were deposited during the cooling limb preceding OIS 82, the peat accumulated in the early part of the warming limb preceding OIS 81, and the Réunion 2 subchron marked the peak of the OIS 82 cold stage (Figure 1). This peat deposit appears to owe its preservation to the fact that after aggradation of this terrace the Maas avulsed to a new course farther west (Figure 7 *a*). Subsequent fluvial incision thus did not occur along the former course, facilitating sediment preservation. A similar instance is also evident near the base of the younger Geertruid 2 terrace (Figure 7 *f*), where a brief interval of normal geomagnetic polarity is evident at the top of the earliest fining-upwards sequence within that terrace[24] (Figure 7 *f*). This has been interpreted as the Cobb Mountain subchron[24], which marked the peak of OIS 36 (Figure 1), indicating that the earliest fining-upward unit within this terrace aggraded during the cooling limb preceding OIS 36. As already noted, this appears to have been the last instance of a geomagnetic instability that was correlated with a maximum in global ice volume.

The pattern interpreted as characteristic of the late Early Pleistocene onwards, of instability in the geomagnetic field occurring during cooling limbs and thus being presumed to mark relatively rapid increases in global ice volume, is well illustrated by the Geertruid 2 terrace. This consists of a ~17 m thickness of fluvial deposits, comprising multiple fining-upwards sand/gravel units deposited within braided channels (Figure 7 *f*). These sediments are thought[20,24] to have been deposited during multiple climate cycles between OIS 36 and 32, such superimposed aggradation being characteristic of the Early Pleistocene in western Europe when uplift rates were low[20,21]. These sands and gravels are overlain by silt that is capped by a humic clay palaeosol and overlain by loess[24]. This clay has yielded pollen indicative of the Bavel 3–5 pollen zones[67], which formed in the later part of the Bavel interglacial (OIS 31; Figure 1). This organic clay has normal geomagnetic polarity (Figure 7 *f*), in contrast with the reversed polarity in the underlying silt. This correlation and the pollen evidence are entirely consistent with the timing of the Matuyama–Jaramillo geomagnetic reversal shortly after the peak of the interglacial in OIS 31, early in the transition to OIS 30, as previously suggested. Since the global ice volume was low at this time, the abrupt fall in VADM that occurred (Figure 2) can be presumed to have accompanied a rapid increase in ice volume. It is also presumed that the start of aggradation of the next terrace in the sequence, the Geertruid 3 terrace (Figure 7 *a*), occurred during the subsequent Heinrich Event in OIS 30, which marked the subsequent rapid increase in VADM (Figure 2). However, this cannot be confirmed at present, because the Geertruid 3 terrace has so far yielded no palaeomagnetic evidence or *in situ* production spike of cosmogenic nuclides.

Conclusions

During the Quaternary, geomagnetic polarity reversals and excursions are well-correlated with interglacial-to-glacial transitions and glacial maxima. It is suggested that this relationship results from interactions between the Earth's mantle and core that accompany decreases in the Earth's moment of inertia during ice accumulation, which weaken the geomagnetic field in order to try to counter the decrease in differential rotation between the mantle and inner core that is being forced. During the Late Pleistocene, geomagnetic excursions directly correlate with brief phases of rapid ice growth, notably during the Younger Dryas stage, following Dansgaard–Oeschger interstadials 5 and 10 that precede the rapid melting events during Heinrich events H3 and H4, and during the transitions between oxygen isotope stages 5c-5b, and 5e-5d. It is proposed that similar relationships between instabilities in climate and the geomagnetic field typefied the Middle Pleistocene, also.

As a result of the transfer of some of the mass of the oceans into polar ice sheets, the climate instabilities that initiate these rapid ice accumulations redistribute angular momentum and rotational kinetic energy between the Earth's mantle and inner core. These changes are shown to weaken the Earth's magnetic field, facilitating geomagnetic excursions and also causing enhanced production of cosmogenic nuclides, including ^{14}C. The subsequent phases of rapid ice melting, Heinrich events, reverse this effect: strengthening the geomagnetic field. This explanation, of forcing of geomagnetic excursions by climate instabilities, provides a natural explanation for why, during the Middle and Late Pleistocene, excursions have been numerous but none has developed into a polarity reversal: the characteristic duration of the climate instabilities is too short for this to be possible.

Past observations of correlations between geomagnetic excursions and other events such as extinctions, may well reflect these rapid climate changes. It is also suggested that river terrace aggradation, in Europe at least, is likely to be concentrated during Heinrich events. The most important Heinrich events can now be dated throughout the Middle and Late Pleistocene, as they are expected to follow the geomagnetic excursions by no more than ~2 ka, thus providing the basis of a method for accurately dating river terrace deposits. Timings of these fluvial aggradations could also be constrained by observation of *in situ* production spikes of cosmogenic

nuclides such as ^{10}Be, which would allow direct correlation with the geomagnetic excursions.

1. Glatzmaier, G. H. and Roberts, P. H., *Science*, 1996, **274**, 1887–1891.
2. Song, X.-D. and Richards, P. G., *Nature*, 1996, **382**, 221–224.
3. Su, W.-J., Dziewonski, A. M. and Jeanloz, R., *Science*, 1996, **274**, 1883–1887.
4. Cox, A., *J. Geophys. Res.*, 1968, **73**, 3247–3260.
5. Gubbins, D., *Geophys. J. Int.*, 1999, **137**, F1–F3.
6. Coe, R. S., Hongre, L. and Glatzmaier, G. A., *Phil. Trans. R. Soc. London*, 2000, **358**, 1141–1170.
7. Olausson, E. and Svenonius, B., *Boreas*, 1975, **4**, 55–62.
8. Doake, C. S. M., *Nature*, 1977, **267**, 415–417.
9. Doake, C. S. M., *Earth Planet. Sci. Lett.*, 1978, **38**, 313–318.
10. Mörner, N.-A., *Danish Meteorol. Inst. Climatol. Pap.*, 1978, **4**, 45–52.
11. Rampino, M. R., *Geology*, 1979, **7**, 584–587.
12. Worm, H.-U., *Earth Planet. Sci. Lett.*, 1997, **147**, 55–67.
13. Valet, J.-P. and Meynadier, L., *Nature*, 1993, **366**, 234–238.
14. Tauxe, L. and Shackleton, N. J., *Geophys. J. Int.*, 1994, **117**, 769–782.
15. Bassinot, F. C., Labeyrie, L. D., Vincent, E., Quidelleur, X., Shackleton, N. J. and Lancelot, Y., *Earth Planet. Sci. Lett.*, 1994, **126**, 91–108.
16. Langereis, C. G., Dekkers, M. J., de Lange, G. J., Paterne, M. and van Santvoort, P. J. M., *Geophys. J. Int.*, 1997, **129**, 75–94.
17. Shackleton, N. J., Berger, A. and Peltier, W. R., *Trans. R. Soc. Edinburgh, Earth Sci.*, 1990, **81**, 251–261.
18. Hilgen, F. J., *Earth Planet. Sci. Lett.*, 1991, **104**, 226–244.
19. Maddy, D., Bridgland, D. R. and Westaway, R., *Quat. Int.*, 2001, **79**, 23–36.
20. Westaway, R., in *River Basin Sediment Systems: Archives of Environmental Change* (eds Maddy, D., Macklin, M. G. and Woodward, J. C.), Balkema, Abingdon, UK, 2001, pp. 87–167.
21. Westaway, R., *Netherlands J. Geosci.*, 2002, **81**, 305–328.
22. Westaway, R., Maddy, D. and Bridgland, D. R., *Quat. Sci. Rev.*, 2002, **21**, 559–603.
23. Tyracek, J., *Sbornik Geologickych Ved. Antropozoikum*, 1995, **22**, 141–157.
24. van den Berg, M. W. and van Hoof, T., in *River Basin Sediment Systems: Archives of Environmental Change* (eds Maddy, D., Macklin, M. G. and Woodward, J. C.), Balkema, Abingdon, UK, 2001, pp. 45–86.
25. Bridgland, D. R. and Allen, P., in *The Early Middle Pleistocene in Europe* (ed. Turner, C.), Balkema, Rotterdam, 1996, pp. 121–134.
26. Bridgland, D. R., *Quat. Int.*, 2002, **92**, 25–34.
27. Antoine, P., *Terra Nova*, 1994, **6**, 453–464.
28. Dansgaard, W. *et al.*, *Nature*, 1993, **364**, 218–220.
29. Keigwin, L. D., Curry, W. B., Lehman, S. J. and Johnsen, S., *Nature*, 1994, **371**, 323–329.
30. Oppo, D. W. and Lehman, S. J., *Palaeoceanography*, 1995, **10**, 901–910.
31. Rasmussen, T. L., Thomsen, E., Labeyrie, L. and van Weering, T. C. E., *Geology*, 1996, **24**, 937–940.
32. Dokken, T. M. and Janssen, E., *Nature*, 1999, **401**, 458–461.
33. Holton, J. R., *An Introduction to Dynamic Meteorology*, Int. Geophys. Ser., Academic Press, San Diego, 1992, vol. 48, p. 511.
34. McIlveen, R., *Fundamentals of Weather and Climate*, Chapman and Hall, London, 1992, p. 497.
35. Glatzmaier, G. H. and Roberts, P. H., *Nature*, 1995, **377**, 203–209.
36. Glatzmaier, G. H. and Roberts, P. H., *Phys. Earth Planet. Int.*, 1995, **91**, 63–75.
37. Glatzmaier, G. H. and Roberts, P. H., *Physica*, Series D, 1996, **97**, 81–94.
38. Glatzmaier, G. H. and Roberts, P. H., *Contemp. Phys.*, 1997, **38**, 269–288.
39. Fairbanks, R. G., *Nature*, 1989, **342**, 637–642.
40. Mitchell, J. and Westaway, R., *Tectonophysics*, 1999, **304**, 157–186.
41. McHargue, L. R., Damon, P. E. and Donahue, D. J., *Geophys. Res. Lett.*, 1995, **22**, 659–662.
42. Kissel, C., Laj, C., Labeyrie, L., Dokken, T., Voelker, A. and Blamart, D., *Earth Planet. Sci. Lett.*, 1999, **171**, 489–502.
43. Laj, C., Kissel, C., Mazaud, A., Channell, J. E. T. and Beer, J., *Phil. Trans. R. Soc. London*, 2000, **358**, 1009–1025.
44. Beck, J. W. *et al.*, *Science*, 2001, **292**, 2453–2458.
45. Baumgartner, S., Beer, J., Masarik, J., Wagner, G., Meynadier, L. and Synal, H. A., *Science*, 1998, **279**, 1330–1332.
46. Fairbridge, R. W., *Nature*, 1977, **265**, 430–431.
47. Mörner, N.-A., *Geology*, 1975, **3**, 109–110.
48. Dreimanis, A. and Goldthwait, R. P., *Geol. Soc. Am. Mem.*, 1973, **136**, 1–71.
49. Mangerud, J., Larsen, E., Longva, O. and Sønstegaard, E., *Boreas*, 1979, **8**, 179–187.
50. Eschman, D. F. and Mickelson, D. M., *Quat. Sci. Rev.*, 1986, **5**, 53–57.
51. Lundqvist, J., *Quat. Sci. Rev.*, 1986, **5**, 269–292.
52. Bowen, D. Q., Rose, J., McCabe, A. M. and Sutherland, D. G., *Quat. Sci. Rev.*, 1986, **5**, 299–340.
53. Masarik, J. and Beer, J., *J. Geophys. Res.*, 1999, **104**, 12099–12111.
54. Sonnett, C. P., Morfill, C. E. and Jokipii, J. R., *Nature*, 1987, **330**, 458–460.
55. Frank, M., *Phil. Trans. R. Soc. London*, 2000, **358**, 1089–1107.
56. Bard, E., Hamelin, B., Fairbanks, R. G. and Zindler, A., *Nature*, 1990, **345**, 405–410.
57. Simpson, J. F., *Geol. Soc. Am. Bull.*, 1966, **77**, 197–204.
58. Hays, J. D., *Geol. Soc. Am. Bull.*, 1971, **82**, 2433–2477.
59. Dubrov, A. P., *The Geomagnetic Field and Life: Geomagnetobiology* (English translation by F. L. Sinclair), Plenum Press, London, 1978, p. 318.
60. Waddington, C. J., *Science*, 1967, **158**, 913–915.
61. von Koenigswald, W. and van Kolfschoten, T., in *The Early Middle Pleistocene in Europe* (ed. Turner, C.), Balkema, Rotterdam, 1996, pp. 211–226.
62. Stuart, A. J., *Biol. Rev.*, 1991, **66**, 453–562.
63. Kopper, J. S., Ph D thesis, Columbia University, 1976.
64. Harrold, F. B., in *The Human Revolution: Behavioural and Biological Perspectives on the Origins of Modern Humans* (eds Mellars, P. and Stringer, C.), Edinburgh University Press, Edinburgh, 1989, pp. 677–713.
65. Ran, E. T. H. and van Huissteden, J., *Meded. Rijks Geol. Dienst.*, 1990, **44**, 209–220.
66. van Andel, T. and Tzedakis, K., *Quat. Sci. Rev.*, 1996, **51**, 481–500.
67. Zagwijn, W. H. and de Jong, J., *Meded. Rijks Geol. Dienst.*, 1983, 37, 155–169.
68. Baksi, A. K., *Geophys. Res. Lett.*, 1995, **22**, 457–460.
69. Cande, S. C. and Kent, D. V., *J. Geophys. Res.*, 1995, **100**, 6093–6095.
70. Channell, J. E. T. and Kleiven, H. F., *Phil. Trans. R. Soc. London*, 2000, **A358**, 1027–1047.
71. Guyodo, Y. and Valet, J.-P., *Nature*, 1999, **399**, 249–252.
72. Singer, B. S., Hoffman, K. A., Chauvin, A., Coe, R. S. and Pringle, M. S., *J. Geophys. Res.*, 1999, **104**, 679–693.
73. Zijderveld, J. D. A., Hilgen, F. J., Langereis, C. G., Verhallen, P. J. J. M. and Zachariasse, W. J., *Earth Planet. Sci. Lett.*, 1991, **107**, 697–714.

ACKNOWLEDGEMENTS. This paper is a contribution to IGCP 449 'Global Correlation of Late Cenozoic fluvial sequences'. I thank Dave Bridgland and Mark White for helpful discussions, and Peter Friend and an anonymous reviewer for thoughtful and constructive reviews.